geoconvention
Virtual Event
September 13 - 15
2021

Reverse time migration approaches for DAS VSP data

Jorge E. Monsegny, Daniel Trad and Don C. Lawton*
University of Calgary and CMC

Summary

Distributed acoustic sensing is a promising technology for seismic monitoring that uses optical fibre as a sensing element instead of geophones. In contrast to geophones, it produces a signal proportional to the strain, or strain rate depending on the vendor, instead of particle velocity. To apply processing techniques, like migration, this strain is usually transformed to particle velocity beforehand. We perform the migration directly in the strain and an associated pressure domains by modifying the wave equation. We compare its results on the reflectivity by using a synthetic model and compare the migration results with data from the Containment and Monitoring Institute Field Research Station. In the synthetic example we obtained a good match between the migrated amplitudes at the reflector depth and the theoretical reflection coefficients. The real data migrations showed a quality similar to the usual path of transforming to vertical particle velocity before migration.

Introduction

The Containment and Monitoring Institute Field Research Station, CAMI-FRS, is a research facility where small volumes of CO2 are being injected annually within a 5 year plan (Lawton et al., 2015; Macquet et al., 2019). In order to monitor the injected CO2 a variety of monitoring technologies are being used there (Lawton et al., 2017).

Distributed acoustic sensing, DAS, is one of those technologies (Mateeva et al., 2013). It consists of an optical fibre used as the sensing element instead of geophones, and an interrogator device that sends light pulses to the fibre and measures the strain or strain rate produced by seismic waves perturbing the fibre from the backscattered light (Hartog, 2018).

Reverse time migration, RTM, is commonly used to create an image of the subsurface using seismic data (Baysal et al., 1983). It has been used to monitor the injection of CO2 using conventional geophone VSP data (Wang et al., 2011). As DAS measures strain, or strain rate, there must be a transformation from DAS to geophone data before performing the RTM. Two usual transformations are Bóna et al. (2017) and Daley et al. (2016).

We perform RTM with DAS data, without transforming it to geophone data, in the strain and pressure domains and compare the results with the usual RTM of geophone data. We find that these two migrations offer a response more proportional to the theoretical reflection coefficients than the particle velocity migration.

Theory

To derive the strain domain and pressure domain RTM for DAS data, we use a staggered acoustic finite difference system in pressure P and particle velocities vx and vz (Liang et al., 2018):

$$\begin{aligned} \frac{\partial P}{\partial t} &= \lambda \left(\frac{\partial v_x}{\partial x} + \frac{\partial v_z}{\partial z} \right) + s \\ \frac{\partial v_x}{\partial t} &= \frac{1}{\rho} \frac{\partial P}{\partial x} \\ \frac{\partial v_z}{\partial t} &= \frac{1}{\rho} \frac{\partial P}{\partial z}, \end{aligned} \tag{1}$$

where the medium properties are density ρ and Lamé parameter λ . The source, s, excites the pressure equation. Figure 1 shows the locations in the staggered grid of the wavefields in the system of equations 1.

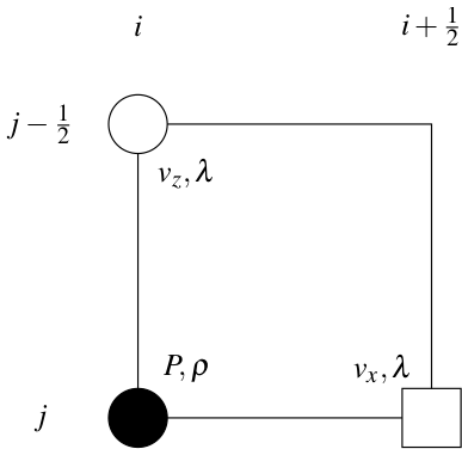

Figure 1: Location of the finite difference wavefields in the staggered grid. Pressure P and density ρ are at integer coordinates (i, j), vertical particle velocity v_z is at coordinates (i, j − 1/2), horizontal particle velocity v x is at (i + 1/2, j) and Lamé parameter λ is defined at both (i, j − 1/2) and (i + 1/2, j).

To link pressure and strain rate, what DAS measures, we use the following identities. In an acoustic medium, the pressure P is related to the normal stresses:

$$-P = \sigma_{xx} = \sigma_{yy} = \sigma_{zz}, \tag{2}$$

while all the shear stresses are zero. In a similar fashion, the normal strains are equal to each other, $\varepsilon_{xx} = \varepsilon_{yy} = \varepsilon_{zz}$, while the shear strains are also zero. Using this, there is a relationship between pressure and normal strain:

$$\begin{aligned} -P &= \sigma_{zz} \\ &= \lambda(\varepsilon_{xx} + \varepsilon_{yy} + \varepsilon_{zz}) + 2\mu\varepsilon_{zz} \\ &= 3\lambda\varepsilon_{zz} \end{aligned} \tag{3}$$

The first RTM transforms the DAS input seismograms from strain rate, f = ∂ εzz , to pressure using equation 3:

$$\begin{aligned} P &= -3\lambda\varepsilon_{zz} \\ &= -3\lambda \int \frac{\partial \varepsilon_{zz}}{\partial t} dt \\ &= -3\lambda \int f dt. \end{aligned} \tag{4}$$

The RTM forward and backward propagations are carried out using the finite difference system of equation 1 with the transformed to pressure seismograms in the backward propagation, part.

The imaging condition is the cross-correlation of forward, P^f, and backward, P^b, pressure wavefields, normalized by the source illumination to diminish migration artifacts and obtain a dimensionless result:

$$I_P(x) = \int_0^{t_{max}} \frac{P^f(x) P^b(x)}{P^f(x) P^f(x)^*} dt. \tag{5}$$

Instead of transforming the DAS seismograms to pressure, we can introduce equation 3 in the finite difference system of equation 1 to obtain a system in strain and particle velocity:

$$\begin{aligned} \frac{\partial \varepsilon_{zz}}{\partial t} &= -\frac{1}{3}\left(\frac{\partial v_x}{\partial x} + \frac{\partial v_z}{\partial z}\right) - \frac{s}{3\lambda} \\ \frac{\partial v_x}{\partial t} &= -3\frac{1}{\rho}\frac{\partial(\lambda\varepsilon_{zz})}{\partial x} \\ \frac{\partial v_z}{\partial t} &= -3\frac{1}{\rho}\frac{\partial(\lambda\varepsilon_{zz})}{\partial z}, \end{aligned} \tag{6}$$

where the locations of each wavefield in the staggered grid is the same as in Figure 1 with ε_{zz} in the place of P.

In this system, we have to calculate spatial derivatives of the product $\lambda\varepsilon_{zz}$. Apart from the additional computational overhead of doing these derivatives, we have to be careful with the discontinuities of λ that can yield immeasurable derivatives and make unstable the system. We use instead a smoothed version of λ to avoid this possibility.

The second RTM starts by turn the DAS seismograms into strain by time integration and filtering of very low frequencies. Similar to the previous RTM, the forward and backward propagations are carried out using the finite difference system of equation 6 using the transformed to strain seismograms in the backward propagation part.

In this case, the imaging condition is the cross-correlation of forward, ε^f_{zz}, and backward, ε^b_{zz}, strain wavefields. Again, we normalize by the source illumination to mitigate migration artifacts and obtain a dimensionless result:

$$I_{\varepsilon_{zz}}(x) = \int_0^{t_{max}} \frac{\varepsilon^f_{zz}(x) \varepsilon^b_{zz}(x)}{\varepsilon^f_{zz}(x) \varepsilon^f_{zz}(x)^*} dt.$$

Results

We are going to do a synthetic experiment to test the response of the pressure and strain migrations showed in the previous section. For that, we are going to follow Chattopadhyay and McMechan (2008) where several imaging conditions are evaluated by migrating data from a two layered model and comparing the resulting migration image along the reflector with the theoretical reflectivities.

Figure 2 shows the velocity model we are going to use in the synthetic experiment. It has two layers and the velocities are close enough to provide a range of precritical reflection angles up to 77°. On the other hand, the density model is constant so it does not influence the reflectivity values. With regard to the survey, it is a single shot gather located at the top left corner of the model while the DAS fibre is located along the surface.

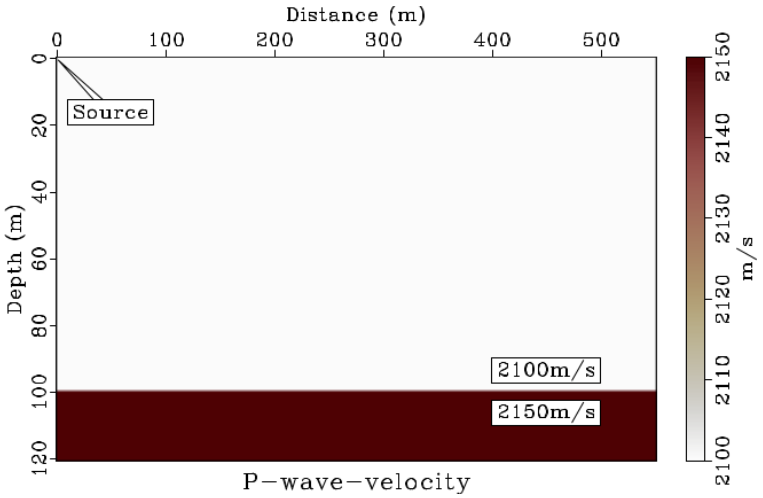

Figure 2: Synthetic experiment velocity model. The velocities follow Chattopadhyay and McMechan (2008) to obtain a range of precritical reflection angles up to 77°. The source is located at the top left corner and the DAS fibre along the surface.

We generated the synthetic data using a finite difference system based on the system of equations 6 and recording the vertical particle velocity, v_z , and vertical strain, ε_{zz}, wavefields at the fibre locations. Figure 3 shows the vertical particle velocity gather on the left and the vertical strain on the middle. The strain rate gather on the right was generated by deriving the strain gather. The direct arrival was muted in all gathers.

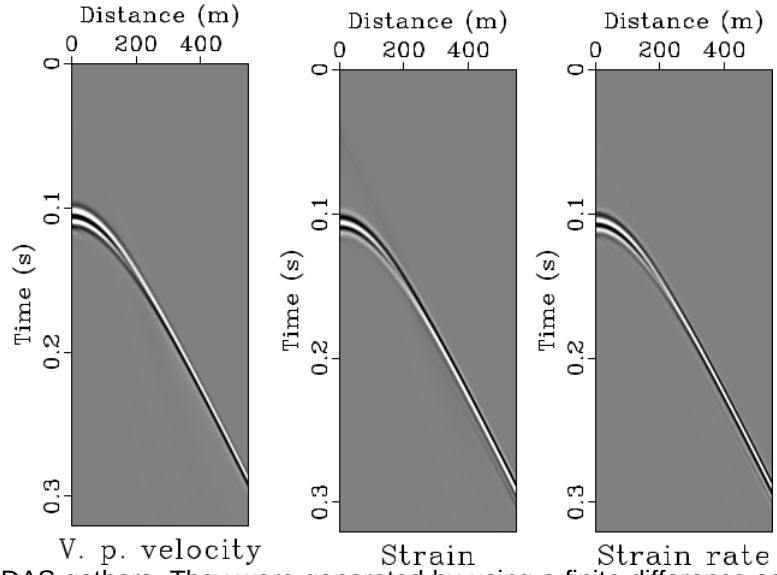

Figure 3: Synthetic DAS gathers. They were generated by using a finite difference scheme based on the system of equations 6. On the left is the vertical particle velocity, v_z, and in the centre is the vertical strain ε_{zz} . The gather on the right is the strain rate and was created by deriving the gather on the middle. The first arrivals were muted.

The Figure 4 shows the migration results. On the left is the vertical particle velocity RTM. On the middle is the pressure RTM with the imaging condition of equation 5. On the right is the corresponding strain RTM with the imaging condition appearing in equation 7.

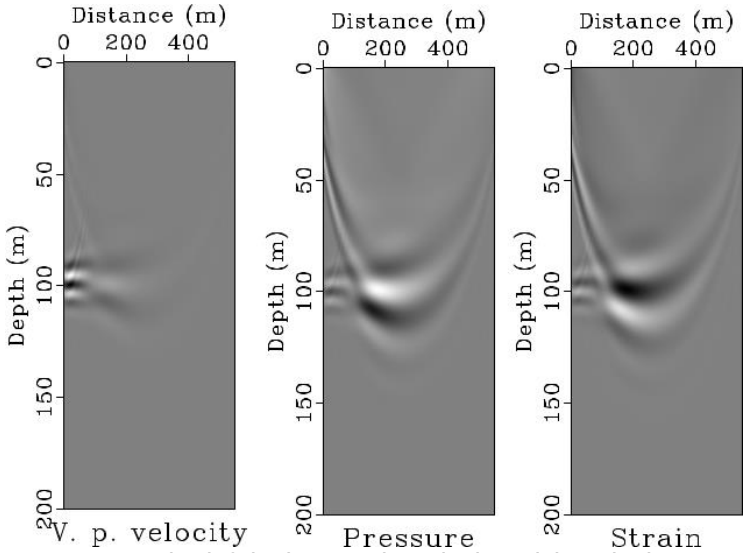

Figure 4: Synthetic data RTM. On the left is the usual vertical particle velocity RTM. On the middle is the pressure RTM obtained by using the imaging condition of equation 5, while on the right is the strain RTM created by using the imaging condition in equation 7.

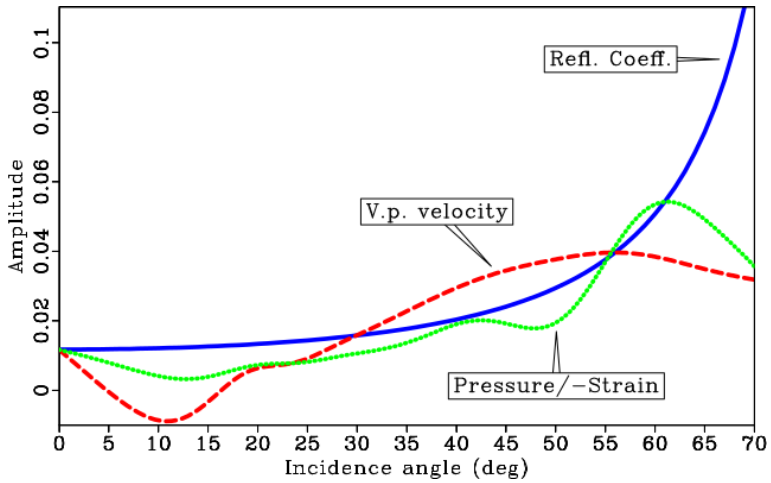

Figure 5: Theoretical geophone reflectivity and amplitudes extracted from the RTM images of Figure 4 at the reflector depth, 100m. The extracted amplitudes were stretched and shifted vertically to match the theoretical curve. Note that we are plotting the extracted amplitude strain with opposite polarity.

In Figure 5 we extracted the amplitudes of the RTM images of Figure 4 at 100m, the reflector depth. As we are interested in the relative amplitudes, we shifted and stretched thesetracted amplitudes to match the theoretical geophone reflection coefficients also plotted on the images. These reflection coefficients were calculated with the usual expression for constant density:

$$R(\theta_1) = \frac{V_1 \cos(\theta_1) - V_2 \cos(\theta_2)}{V_1 \cos(\theta_1) + V_2 \cos(\theta_2)}, \tag{8}$$

where V 1 is the velocity of the top layer, V 2 the velocity of the bottom one, θ1 is the incidence angle and θ2 is the refraction angle that is related to θ1 by Snell's law. In Figure 5, notice that we plot the strain amplitude with the opposite polarity and that it is practically identical to the pressure amplitude plot.

We also tested the pressure and strain migrations using real DAS data. The data is from a walkaway VSP survey acquired at CaMI-FRS. It is composed of 17 shot gathers around the well.

This data contains only the upgoing events and its processing consisted of geometry, first break picking, wavefield separation, gain for spherical transmission and loss, and deconvolution of the upgoing wavefield (Gordon, 2019).

The Velocity and density models were scaled down from well log data and extended horizontally. The top 35m of the P-wave velocity model were obtained by a first arrivals tomography.

A spectral analysis of DAS data revealed that most of the frequencies are in a zone between 50Hz and 150Hz. For this reason, a 100Hz Ricker wavelet was used as the source in the migrations as an approximation of a Klauder wavelet that is usually used in data produced by vibrational sources.

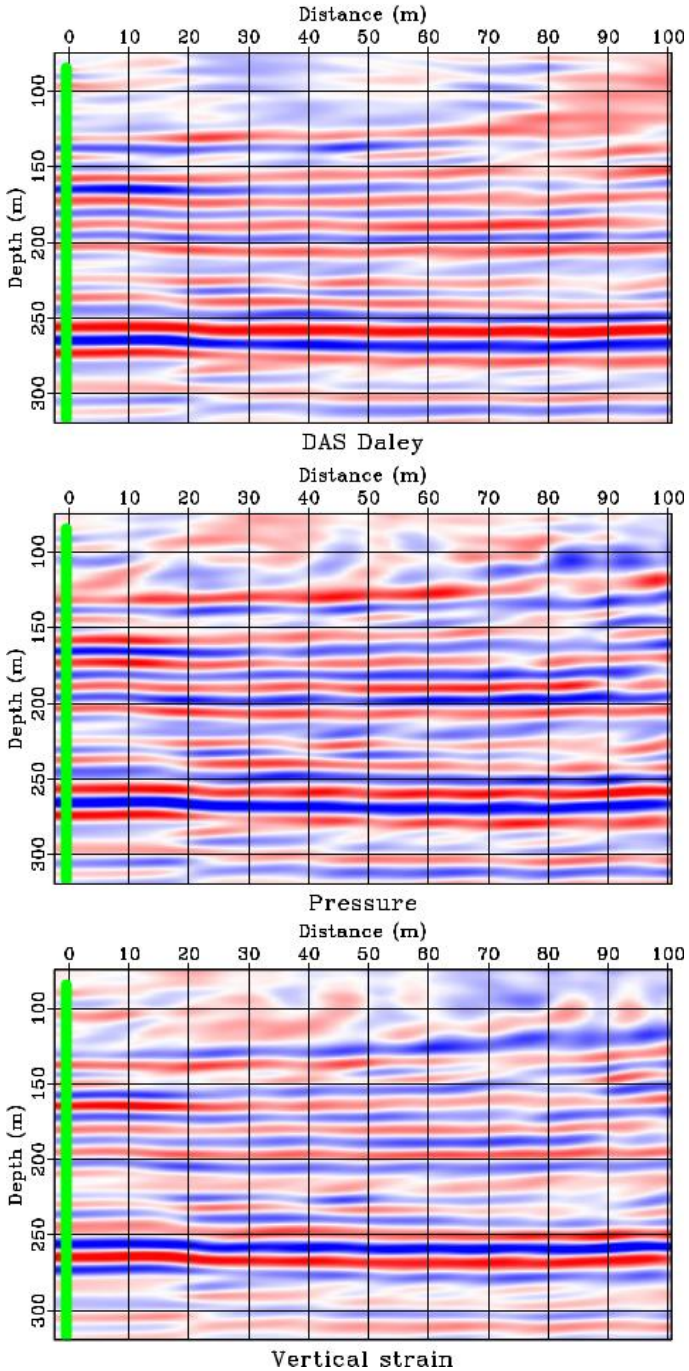

Figure 6: VSP DAS migrations with data from CaMI-FRS. Top shows the usual workflow that first turns the DAS data into geophone data by using the method of Daley et al. (2016) and then preforms a particle velocity migration. Middle is the pressure RTM and bottom is the strain RTM.

Finally, Figure 6 displays the reverse time migrations of the CaMI-FRS DAS VSP data. The top shows the usual RTM of DAS data that first transforms the data into vertical particle velocity using the method of Daley et al. (2016) and then performs a particle velocity RTM. In the middle is the

pressure RTM for DAS data and in the bottom is the strain RTM for DAS data described before. The pressure and strain RTM images offer a similar quality than the usual RTM. Also, as noticed before in the synthetic example, Figure 5, the strain RTM has the opposite polarity of the pressure RTM.

Conclusions

Two reverse time migrations for strain and pressure data, more natural to DAS, data were developed.

The synthetic test showed that the relative amplitudes obtained with the strain and pressure migrations is similar to the theoretical reflectivities, so not only the kinematic behaviour of the reflectors can be produced but also the dynamic one.

The real data test showed that the strain and pressure migrations have a similar quality to the migration of DAS data converted to particle velocity. This means that this kind of imaging can be done directly with DAS data without applying a transformation.

Acknowledgements

We thank the sponsors of CREWES and the CaMI.FRS JIP subscribers for continued support. This work was funded by CREWES industrial sponsors and CaMI.FRS JIP subscribers, NSERC (Natural Science and Engineering Research Council of Canada) through the grants CRDPJ 461179-13 and CRDPJ 543578-19. The authors also acknowledge financial support from the University of Calgarys Canada First Research Excellence Fund program: the Global Research Initiative in Sustainable Low-Carbon Unconventional Resources. The data were acquired at the Containment and Monitoring Institute Field Research Station in Newell County AB, which is part of Carbon Management Canada.

References

Baysal, E., D. D. Kosloff, and J. W. C. Sherwood, 1983, Reverse time migration: GEOPHYSICS, 48, 1514–1524.

Bóna, A., T. Dean, J. Correa, R. Pevzner, K. Tertyshnikov, and L. Zaanen, 2017, Amplitude and phase response of DAS receivers: Presented at the 79th EAGE Conference and Exhibition 2017.

Chattopadhyay, S., and G. A. McMechan, 2008, Imaging conditions for prestack reverse-time migration: GEOPHYSICS, 73, S81–S89.

Daley, T., D. Miller, K. Dodds, P. Cook, and B. Freifeld, 2016, Field testing of modular borehole monitoring with simultaneous distributed acoustic sensing and geophone vertical seismic profiles at Citronelle, Alabama: Geophysical Prospecting, 64, 1318–1334.

Gordon, A. J., 2019, Processing of DAS and geophone VSP data from the CaMI Field Research Station: Master's thesis, University of Calgary.

Hartog, A. H., 2018, An introduction to distributed optical fibre sensors: CRC Press.

Lawton, D., M. Bertram, K. Hall, and K. Bertram, 2015, New approaches to seismic monitoring at the Brooks Field Research Station: Technical report, CREWES.

Lawton, D., M. Bertram, A. Saeedfar, M. Macquet, K. Hall, K. Bertram, K. Innanen, and H. Isaac, 2017, DAS and seismic installations at the CaMI Field Research Station, Newell County, Alberta: Technical report, CREWES.

Liang, W., X. Wu, Y. Wang, and C. Yang, 2018, A simplified staggered-grid finite-difference scheme and its linear solution for the first-order acoustic wave-equation modeling: Journal of Computational Physics, 374, 863 – 872.

Macquet, M., D. C. Lawton, A. Saeedfar, and K. G. Osadetz, 2019, A feasibility study for detection thresholds of CO2 at shallow depths at the CaMI Field Research Station, Newell County, Alberta, Canada: Petroleum Geoscience, 25, 509–518.

Mateeva, A., J. Lopez, J. Mestayer, P. Wills, B. Cox, D. Kiyashchenko, Z. Yang, W. Berlang, R. Detomo, and S. Grandi, 2013, Distributed acoustic sensing for reservoir monitoring with vsp: The Leading Edge, 32, 1278–1283.

Wang, Y., L. Huang, and Z. Zhang, 2011, Reverse-time migration of time-lapse walkaway vsp data for monitoring co2 injection at the sacroc eor field: SEG Technical Program Expanded Abstracts 2011, 4304–4308.